Manufacturing Science and Technology 3(4): 98-105, 2015 http://www.hrpub.org
DOI: 10.13189/mst.2015.030403

Multilayer Graphene (MLG)-Reinforced Al_2O_3 Nanocomposites Fabricated by High-frequency Induction-heat Sintering Technology

I. Ahmad

Center of Excellence for Research in Engineering Materials - Advanced Manufacturing Institute, King Saud University, Kingdom of Saudi Arabia

Abstract Nanocomposites of Al_2O_3 (alumina) ceramic reinforced with various multilayer graphene (MLG) contents (2 and 4 vol.%) were fabricated by novel rapid high-frequency induction-heat (HF-IF) sintering technology and their microstructures, interface and mechanical properties were meticulously investigated. MLG was synthesized through thermal exfoliation process and dispersed homogenously into Al_2O_3 matrix by colloidal chemistry technique. Novel HF-IF sintering consolidated nanocomposites to 99% relative densities without damaging the MLG nanostructures and contributed in forming good Al_2O_3/MLG interface. The fracture toughness (K_{IC}) of the nanocomposites was increased by 41% and 25% whereas a 6% increase and 15% reduction in hardness values were observed at 2 vol.% and 4 vol.% MLG additions respectively, compared to unreinforced Al_2O_3. Rise in the K_{IC} values of the nanocomposites was associated with, (i) higher densities due to novel HF-IH sintering, (ii) uniform dispersions of the MLG within Al_2O_3 matrix, (iii) fracture-mode alteration, (iv) grain refinement, (v) strong MLG/Al_2O_3 interface and (vi) MLG/Al_2O_3 grain bridging and grain sharing toughening mechanism.

Keywords Multilayer graphene (MLG), Nanocomposite, Al_2O_3, Microstructure, Interface

1. Introduction

Graphene is 2D nanosheets of carbon atoms and is the stiffest and strongest carbon based nanomaterial and offer ceramics/polymer/metallic matrices for becoming super strong materials provided that the unique properties of graphene nanostructures could be transferred to the resulting nanocomposites [1,2]. Multifunctional nanocomposites are the hottest topic in contemporary materials because these are suitable as structural materials and also satisfy the needs for additional functionality requirements such as electrical, magnetic, optical, chemical, biological etc. Although, graphene can be promising contestant for converting the brittle ceramics into superior structural material, however less focused [3].

Alumina (Al_2O_3) is an attractive ceramic for advanced high temperature structural applications and is currently used in electronics, aerospace and automotive industries [4-8]. Despite inspiring mechanical hardness and chemical inertness, the poor fracture toughness restricts Al_2O_3 use for advanced structures of aircraft engine, rocket materials, armor materials, automobiles and other space engineering applications [9].

It is widely suggested that carbon based nanomaterials have capability to curtail the Al_2O_3 brittleness and strong/elastic CNTs have extensively been reinforced into Al_2O_3 for this purpose. [10-18]. Literature indicates that the CNTs agglomerations, nanocomposites densification and weak interfacial Al_2O_3/CNTs connections are big challenges [10-22] thus the potentials of CNTs could still not be fully utilized into Al_2O_3.

In contrast with CNTs, graphene offers higher specific surface area, mechanical strength/flexibility, fewer tendencies to tangle thus dispersion is far easy into a ceramic matrix, high yield [23-25]. Therefore, the graphene has potentials to substitute CNTs for preparing tougher Al_2O_3 nanocomposites. Walker *et al.* reported impressive 235% higher in K_{IC} of Si_3N_4 after loading with 1.5 vol.% graphene whereas Dusza *et al*. could get moderate 45% increase at 3.0 vol.% graphene additions into Si_3N_4, compared to monolithic samples [26,27]. Moderate K_{IC} improvements of 27%, 28% 33%and 53% in Al_2O_3 ceramic after 0.3 vol.%, 0.8 vol.%, 0.22 wt.% and 2 wt.% graphene loadings have been reported [28-30]. It is fact that graphene is an effective nano-reinforcement to enhance mechanical performance of the Al_2O_3 ceramics. Furthermore, thin graphene, quality distribution into base matrix, novel rapid sintering process and firm graphene/Al_2O_3 interface could further upgrade

Al_2O_3 for structural part, thus interesting [31].

In this perspective, we prepared highly dense Al_2O_3 nanocomposites reinforced with various MLG contents (2 vol.% and 4 vol.%) using HF-IH sintering technology. The resulting nanocomposites were systematic investigated for structural analysis and mechanical properties evaluation. The leading objective of this study is to introduce HF-IH sintering, as a promising technique, for producing quality graphene-reinforced Al_2O_3 nanocomposites. Fast HF-IH sintering indeed facilitated to form strong MLG/Al_2O_3 interfacial connections and to retain the graphene nanostructures into nanocomposites thus better mechanical properties could be attained in the final nanocomposites.

2. Materials and Experimental Methods

2.1. Nanocomposites Preparation

Three-Dimensional graphite flakes (grade 3775-Asbury Graphite Mills, Inc., New Jersey, USA) were chemically modified to graphite oxide (GO) by process, as described in the Hummers method and others [32]. Subsequently, the thermal exfoliation of the GO was performed at 1800°C using a heating rate higher than 1000°C/min under high vacuum conditions to produce thin MLG [33]. For obtaining uniform MLG dispersion into the base matrix, a colloidal chemistry technique was opted and for this purpose, designed amounts of MLG (0.2 g) were added into distilled water (100 ml) and small amounts of sodium dodcyle sulfate (SDS, < 2 wt.% of the MLG) was also added. The aqueous MLG/SDS slurry was agitated with the assistance of ultra-sonic probe (Sonic Vibracell, VCX-750, manufactured by Sonics, Materials Incorporation, USA, power 750 watts, frequency 20 KHz) for 30 min and sufficient time (2 week) was given to slurry for thorough adsorption of SDS on MLG surface and again sonicated for 30 min. A separate slurry of aqueous/Al_2O_3 nanopowder (Sigma Aldrich, UK having particle size < 30 nm) was also prepared and later both suspensions were mixed and ultrasonicated for 60 minutes and dried at 120°C. The dried nanocomposite were condensed by HF-IH sintering furnace (Korea) at 1500°C at a heating rate of 150°C/min under an uniaxial pressure of 50 MPa and high vacuum (4.5×10^{-2} Tor) and the temperatures were consistently monitored by an optical pyrometer (Thermalert TX, Raytek GmbH, Germany). Pure monolithic Al_2O_3 reference samples were also fabricated following the same processing conditions.

2.2. Physical Properties and Material Characterization

Well-known Archimedes method was adopted to measure the apparent densities of all sintered nanocomposites samples. For relative density assessment the theoretical densities of 3.9 g/cm^3 for Al_2O_3 and 2.1 g/cm^3 for MLG were used [26,34]. Bruker D-8 Discover X-ray diffractometer using Cu Kα radiation, Germany was utilized to identify the phases present in the sintered samples. Structural features and grain size was analyzed by scanning electron microscope, SEM, (FEG-SEM JEOL JSM-7600F, Japan.). Fractured and polished/thermally etched, at 1400 °C for 15 min in inert atmosphere, were prepared for observation under SEM. For structural examination of MLG and interfacial investigations of the MLG/Al_2O_3 nanocomposites, an advanced transmission electron microscope, TEM, (FEG-TEM 2100F, JEOL, Japan) was used. For TEM analysis, MLG sample was prepared by dispersing MLG into acetone and later transferred to holey-carbon TEM grid. For interfacial investigation, sintered nanocomposite samples were prepared by ion milling technology using ion–slicer (EM 09100 IS, JEOL, Japan).

2.3. Mechanical Testing

Microhardness of all polished sintered samples were measured at 9.8 N loads for 15s employing Buehler-micromet 5114 (Akashi corporation, Japan) and later the obtained Vickers hardness numbers (*HV*) were further converted to GPa [21]. Nanoindentation technique was adopted to determine the nanohardness and elastic modulus of all sintered samples. Nanoindentation measurements were performed using a NanoTest, (Micro Materials, and UK). The indenter was continuously loaded to peak load of 200 mN in 25-30 sec and unloaded after holding time 30 sec to allow full plastic deformation. Reduced modulus was directly obtained from machine whereas the modulus of elasticity was calculated by employing equation-1 [35].

$$E = \frac{[1-Vs^2]}{\left[\frac{1}{E_r}-\frac{\{1-Vi^2\}}{E_i}\right]} \quad (1)$$

where *Vs* and *Vi* are the Possion's ratio of the test piece (0.23 for monolithic Al_2O_3 and composites) and the indenter (0.07 for diamond) respectively, *Ei* is the elastic modulus of the indenter (1.14×10^6 Nmm^{-2} for diamond).

The K_{IC} of all samples was appraised using the direct crack measurement (DCM) method, the lengths of crack emerging from the corner of an indent generated during Vickers hardness tests were used to estimate the K_{IC}. The crack lengths were carefully measured using SEM and the recorded images were analyzed using images processing and analysis software (Image). The K_{IC} value was calculated using equation-2 [36].

$$K_{IC} = 0.016\left(\frac{E}{H}\right)^{\frac{1}{2}}\left(\frac{P}{C^{\frac{3}{2}}}\right) \quad (2)$$

where *E* is the modulus of elasticity, *H* is the micro-hardness (HV) and *c* is the radial crack length generated by the Vickers indentation. 10 indents were made on each sample.

3. Results and Discussions

3.1. MLG Synthesis and Dispersions

Electron microscopy revealed interesting structural features concerning (i) the quality of the MLG prepared by thermal exfoliation process and (ii) the homogenous dispersion of MLG within the base Al_2O_3 matrix. SEM studies of the thermally exfoliated MLG, **Figure 1a**, showed two-dimensional sheet-like geometrical features associated with the MLG and the close observation of a MLG edge was appeared with nanometric dimension (~ 6 nm), as shown in **Figure 1b**. Furthermore, light contrast of the same MLG samples under TEM depicts thin or mono graphene sheet (white arrow) whereas relatively darker contract represents fewer MLG layers (black arrow) and the crumpling or wrinkling of thin MLG (black arrow) was also observed, as exhibited in **Figure 1c**.

The thermal reduction of GO is entirely a complex mechanism and the GO has to undergone stern chemical processes (eradication of the intercalates *i.e.* H_2O molecules and oxides groups) and rigorous physical phenomenon (folding/unfolding and reshuffling of individual graphene layers), at the instant of rapid thermal shock, before its transformation to thin MLG, as already proposed [37]. These obvious microscopic details suggest that graphene maintained its two-dimensional sheet morphology, structure and nanoscale features throughout elevated temperatures exfoliation process.

Uniform distribution of MLG within the Al_2O_3 grains is important to prepare superior quality nanocomposites. SEM fractured surfaces of the sintered samples in **Figure 2b** clearly shows the homogenously dispersion of MLG (black arrows) within the Al_2O_3 grains. Indeed combined processing of ultrasonication, surfactant and time provided for surfactant adsorption to MLG surfaces jointly contributed in obtaining the uniform distribution of MLG within the parent ceramic matrix. Ultrasonication provided high energy sonic waves to detangle the MLG and the surfactant adsorbed on the MLG surfaces to create positive electrostatic repulsive force with each others to counter the Van der Waal attractions for even distributions of MLG within Al_2O_3 nanoparticles [26].

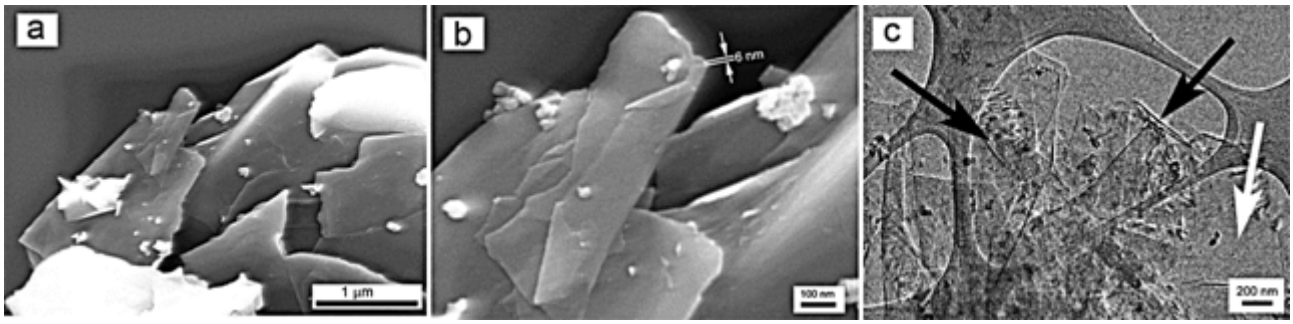

Figure 1. SEM images of thermally exfoliated MLG at (a) low magnification, showing stacks of MLG, (b) high magnification, showing the thinness of the MLG and (c) TEM image of thermally exfoliated MLG.

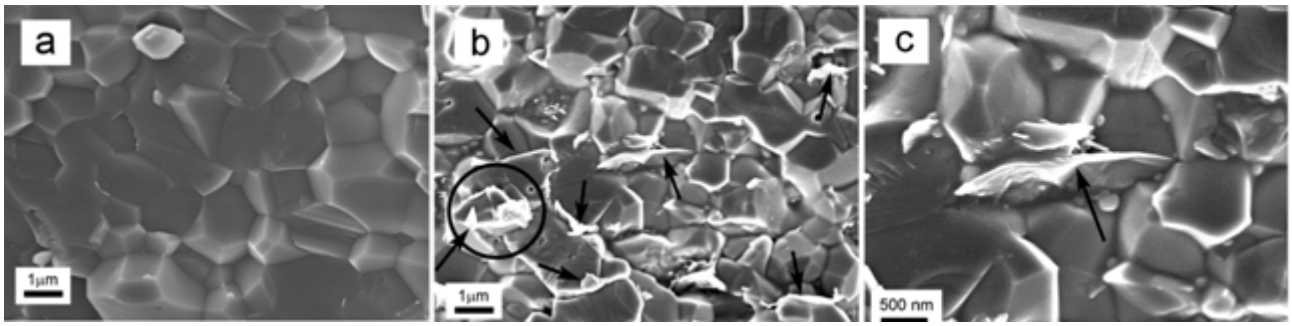

Figure 2. SEM images of the fractured samples of (a) monolithic Al_2O_3, (b) Al_2O_3-MLG nanocomposites samples showing the homogenous dispersions of MLG (black arrows) and wrapping of MLG (black circle) around Al_2O_3 matrix grain and (c) MLG pull-out (black arrow) in the nanocomposites samples.

3.2. Densification and Structural Features

Novel HF-IH sintering consolidated monolithic Al_2O_3 to near theoretical densities (99.9%) however, additions of MLG (2 vol.% and 4 vol.%) resulted in minor decrease (0.5 and 1%) in the densities of nanocomposites, respectively as graphically represented in **Figure 3**. This indicates that novel sintering technique, owning rapid heating rate, simultaneous pressure application and short sintering duration, is promising to condense MLG/Al_2O_3 nanocomposites to higher densities [38].

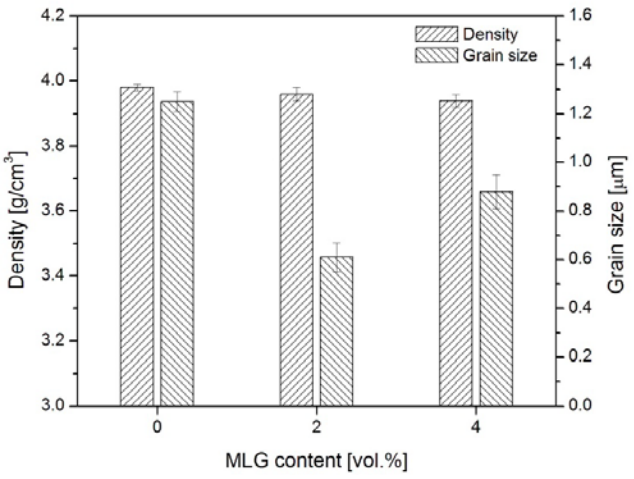

Figure 3. Density and grain size profiles of monolithic Al_2O_3 as function of MLG additions.

The novel HF-IH sintering process is done in a graphite die, somehow like hot pressing, but the heating is performed by a source of high-frequency electricity to drive a large alternating current through a copper (Cu) coil, around the graphite die. When the current is passed through this coil, a very intense and rapidly changing magnetic field is generates in the space within the work coil. The conductive graphite die containing ceramic composite powder is placed within this intense alternating magnetic field which induces a current flow in the conductive graphite die. Thus allows the right amount of heat for desired period of time which surely ensures controlled performance without damaging the MLG nanostructure and consolidate nanocomposite to higher densities [39]. **Figure 2b** also shows that the MLG are wrapped around (black circle) the grain boundaries and this might be the another reason behind the grain refinement effect in the nanocomposites because MLG existing around the grain boundaries can effectively prevent the grain growth during sintering, and act as pining points to slow down grain boundary movement during grain growth in consolidation process [28]. However, further addition on MLG barely influenced the grain size and this could be due to the agglomeration of MLG at high concentration (black arrow in **Figure 4c**), as getting homogenous dispersions of MLG at concentration greater than 2 vol.% is challenging. It means that MLG merely accumulate at grain boundaries rather than pinning them thus further reduction in grain size could not be obtained, as demonstrated graphically in **Figure 3** and structurally **i**n **Figure 4**.

3.3. Fracture Toughness (K_{IC}) and other Mechanical Properties

The K_{IC} values of all monolithic Al_2O_3 and MLG-reinforced Al_2O_3 nanocomposites samples were estimated by direct crack method (DCM), as adopted in several nanocomposites studies [13,16,18,19,20]. Compared to monolithic Al_2O_3, a 47% and 25% rise in K_{IC} values was obtained in nanocomposites samples containing 2 vol.% and 4 Vol.% MLG respectively, as shown in **Figure 5a**. **Figure 5b** represents a respective increase of 7 % hardness at 2 vol.% MLG whereas 18% decrease in hardness was recorded for composite containing 4vol.% MLG against monolithic Al_2O_3. With reference to benchmark monolithic Al_2O_3, 0.6% and 3% reductions in elastic modulus were also noticed for nanocomposites reinforced with 2 vol.% and 4 vol.% MLG contents, respectively.

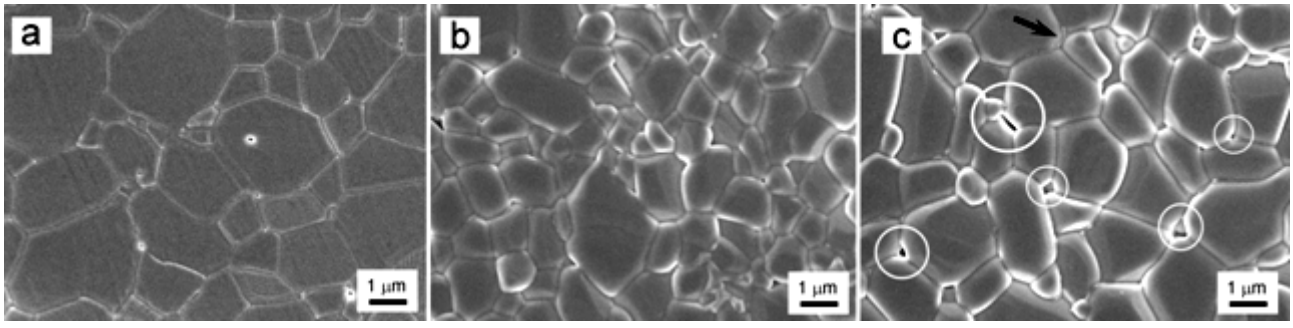

Figure 4. SEM images of the thermally etched (a) monolithic Al_2O_3 exhibiting coarse/ prismatic grains, (b) Al_2O_3-2 vol.% MLG nanocomposites shows fine-grained microstructure and (c) Al_2O_3-4 vol.% MLG nanocomposites shows porosity (white circles), MLG glut (black arrow) and blunt grain shape.

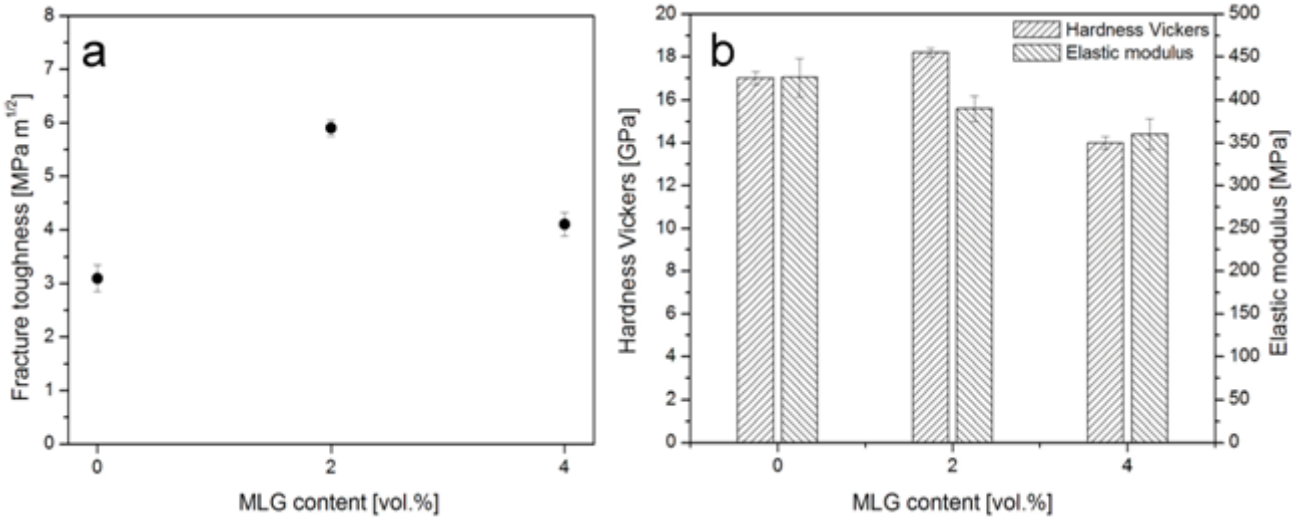

Figure 5. Effects of MLG contents on (a) the K_{IC} and (b) hardness and elastic modulus of the monolithic Al_2O_3.

SEM investigations of the fractured surfaces of samples greatly helped in understanding the reasons behind the hike in fracture toughness, as shown in **Figure 2**. The freshly fractured nanocomposites samples showed interesting features which explained that the conventional toughening mechanisms derived for fiber reinforced composites are also applicable to Al_2O_3-MLG nanocomposites [21]. MLG grain sharing (**Figure 6a**) MLG pull-out (**Figure 2a**) and crack bridging (**Figure 6b**) mechanisms were also observed in fractured samples and these exiting toughening mechanisms are believed to have vital role in improving the K_{IC} of the nanocomposites. Furthermore, **Figure** 6a shows that the MLG is perfectly embedded within the two Al_2O_3 grains thus strengthened the grain boundaries and led to the changed the fracture mode, from intergranular in case of monolithic Al_2O_3 (**Figure 2a**) to mixed inter/intra transgranular in the nanocomposites (**Figure 2b**). It is further that noted in **Figure 2b** that a large GNP securely wrapped/rolled around the Al_2O_3 grain (black circle), possibly due to their flexibility and high aspect ratio, forming a large area of interface with matrix. This unique interaction associated with the two-dimensional geometry of the MLG generated anchoring mechanism which can lead to increased interfacial frictions between the MLG and the matrix, and increase the required energy to pull out such MLG. Therefore, the fracture accrued through the Al_2O_3 grains rather than grain boundaries, as demonstrated in **Figure 2b**. These results mean that the MLG have played significant role in improving the fracture toughness, due to their distinctive microstructures by (i) increasing the required pull out energy during fracture (ii) anchoring around the Al_2O_3 grains and (ii) producing higher contact area with grains. The nominal differences in the hardness and elastic modulus are possibly due to the graphene layer sliding in MLG during the course of deformation [23].

In ceramic materials, the grain size and grain morphology define the mechanical properties. High hardness value of monolithic Al_2O_3 may be attributed with the elongated prismatic and needle-like grain shapes, as shown in **Figure 4a**. After addition of 2 vol.% MLG, no apparent change in the microstructure was observed except grain size reduction (see **Figure 4b**). It means that MLG has induced more grain boundaries by refining matrix microstructure. It is fact that grain boundary area and reinforcing constituents mutually hinder the onset of plasticity by impeding dislocation movement across the entire nanocomposite microstructure [34] thus led composites containing 2 vol.% MLG to a respective hike of 7 % and 45 % in hardness and K_{IC} values, against unreinforced Al_2O_3. In contrast, an 18% reduction in hardness along with deprived K_{IC} values were noticed in Al_2O_3/4 vol.% MLG sample, as shown in **Figure 5a**. This drop in mechanical properties of the nanocomposites containing higher MLG additions may be associated with change in grain shape, intrinsic lubrication characteristics of graphene and residual porosity, as appeared in the composite microstructure shown in **Figure 4c**. Compared with monolithic alumina blunt/round grains morphology was noticed in the Al_2O_3/4 vol.% MLG nanocomposites, **Figure 4c**, and presumably this phenomenal change has facilitated sliding of the grains over each other because the rounded grains could easily slide on each others compared to faceted ones [40]. Furthermore, the residual porosity (white arrows in **Figure 4c**) in the microstructure of the Al_2O_3/4 vol.% MLG nanocomposites could be another factor in declining hardness and K_{IC} values because the ceramics are sensitive to residual porosity according to an empirical square root relationship ($\sigma_F \propto l^{-0.5}$) which describes the fracture strength (σ_F) dependency on the pore size (c) [34]. Most probably the residual porosity would have facilitated the crack to initiate at much lower load thus nanocomposites has lower mechanical performance [34]. Adding on, Figure 5b also shows consistent drop in the elastic modulus (E) values of the nanocomposite samples with increasing MLG concentration. This decrease is elastic modulus is probably due to the presence of porous features and low modulus of the large MLG along both in-plane and out-of-plan directions, as suggested in earlier study [41].

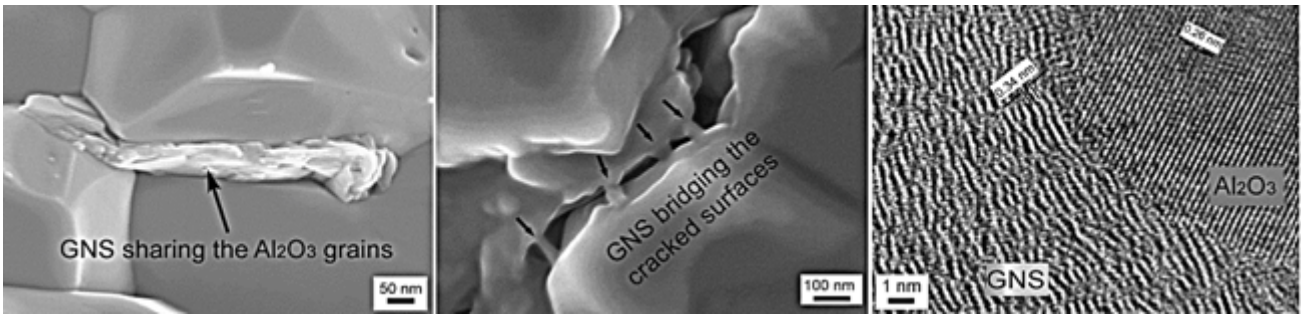

Figure 6. High resolution SEM images of fractured surfaces of nanocomposites samples showing (a) grain sharing phenomenon, (b) crack-bridging phenomenon and high resolution lattice resolved TEM images of nanocomposite showing the Al_2O_3/MLG interface.

3.4. Interfacial Investigations

Existence of a sturdy interface between the Al_2O_3 and the MLG is imperative to transfer the exceptional mechanical properties of MLG to the nanocomposite for performing unique toughening mechanism. During loading sequence, weakly bonded MLG with Al_2O_3 would pull-out easily without transferring the load from one Al_2O_3 grain to another resulting in nanocomposite with meager mechanical performance. In depth atom level study of the nanocomposites by TEM is greatly helpful in revealing the interfacial details exist at Al_2O_3/MLG junctions. **Figure 6c** shows high-resolution lattice resolved TEM images where MLG with typical fringe separation of 0.34nm which corresponds to the graphitic (002) planes of MLG can be indentified and Al_2O_3 can be recognized by its fridge distance of 0.26nm corresponds to (104) planes. In earlier studies, the formation of a strong connection at the Al_2O_3/CNT interface through an intermediate thin phase (Al_2OC) has been reported [18,19].

Nevertheless, both the CNT and MLG are constituted by graphitic structure however, our FEG-TEM investigation reveals that MLG is directly adhere with the Al_2O_3 without any intermediate phase. The reported interface in case of Al_2O_3/CNT is probably due the long duration sintering process *i.e.* hot-pressing which possibly allowed CNT/Al_2O_3 to form an intermediate phase through slow diffusion mechanism [18]. In contrast, novel HF-IH technology adopted in this study is a rapid sintering technology and the sintering mechanism is entirely different (creep and related mechanisms) from the conventional (diffusion and mass transportation of materials across grain boundaries) sintering processes [18,38,39]. Absence of any interfacial second phase layer between MLG and Al_2O_3 strongly suggests direct atomic level attachment between the MLG and Al_2O_3 matrix, as shown in **Figure 6c** (white arrow). Based on the TEM results, strong MLG/Al_2O_3 interfacial connections is suggested which allow MLG to play a direct contribution in absorbing more energy during crack propagations and led nanocomposite to higher toughness.

4. Conclusions

- In this repot, novel rapid high-frequency induction-heat (HF-IF) sintering technology was used to fabricate Al_2O_3 (alumina) ceramic nanocomposites reinforced with 2 vol.% and 4 vol.% of the MLG contents. The resulting nanocomposites were appraised for structural investigation and mechanical properties evaluation by employing diverse analytical techniques.
- The natural graphite was chemically reduced to prepare graphite oxide (GO) and then transferred to thin MLG by thermal exfoliation process. Electron microscopic investigation confirmed the preparation of very thin (~ 6 nm) graphene nanosheets (MLG). Later these MLG were evenly distributed into Al_2O_3 ceramic matrix by adopting colloidal chemistry method.
- New HF-IF sintering route, practiced in this study, provided several benefits such as (i) condensed the monolithic Al_2O_3 and nanocomposites to > 99% relative sintered densities, (ii) short sintering duration protected the nanostructures of MLG from degradation by retaining its morphology/structure and (iii) contributed in forming strong Al_2O_3/MLG interfacial connections.
- Structurally, 50% and 35% refinement into the grain size of monolithic Al_2O_3 was obtained at the MLG loading of 2 vol.% and 4 vol.% respectively. Further, the incorporation of MLG altered the fracture mode from intergranular in monolithic Al_2O_3 to mixed inter/transgranular in the nanocomposites.
- Mechanically, the K_{IC} of the nanocomposites was increased by 45% and 25% whereas 7% increase and 15% drop in hardness values was recorded at 2 vol.% and 4 vol.% MLG additions respectively, compared to unreinforced Al_2O_3.
- Rise in the K_{IC} of the nanocomposites was associated with, (i) higher densities due to novel HF-IH sintering, (ii) uniform dispersions of the MLG within Al_2O_3 matrix, (iii) fracture-mode alteration, (iv) grain refinement, (v) strong MLG/Al_2O_3 interface and (vi) grain bridging/grain sharing toughening mechanism in MLG/Al_2O_3 nanocomposites.

Acknowledgements

This work was financially supported by center of excellence for research in engineering materials (CEREM), Advanced Manufacturing Institute (AMI), King Saud University, Kingdom of Saudi Arabia. Authors are grateful to all technical staff of CEREM labs for their help in material characterization, nanoindentation and high–frequency induction heat sintering.

REFERENCES

[1] K. S. Novoselov, A. K. Geim, S. V. Morozov, D. Jiang, Y. Zhang, S. V. Dubonos, I. V. Grigorieva and A. A. Firsov, Electric field effect in atomically thin carbon films, *Science*, 306 (2004), 666-669.

[2] S. Bai, and X. Shen, Graphene-inorganic nanocomposites, *RSC Advances*, 2 (2012), 64-98.

[3] H. Shifeng and C. Xin, Effect of carbon black on properties of 0-3 piezoelectric ceramics/cement composites, *Current Applied Physics*, 9 (2009), 1191-1194.

[4] K. Niihara, New design concept of structural ceramics-ceramics nanocomposites. *J. Ceram. Soc. Japan*, 99 (1999), 974-982.

[5] Centeno, V.G. Rocha, B. Alonso, A. Fernández, C.F. Gutierrez-Gonzalez, R. Torrecillas and A. Zurutuza, Graphene for tough and electroconductive alumina ceramics, *J. Eur. Ceram. Soc*., 33 (2013), 3201–3210.

[6] Y. Wu, X. Zhang and J. Guo, Microstructural development and mechanical properties of self-reinforced alumina with CAS addition, *J. Eur. Ceram. Soc.*, 2 (2001), 581–587.

[7] A. G. Evans, Perspective on the development of high-toughness ceramics, J. *Am. Ceram. Soc.*, 73 (1990), 187-206.

[8] J. R. Martinlli and F. F. Sene, Electrical resistivity of ceramic–metal composite materials: application in crucibles for induction furnaces, *Ceram. Int.*, 26 (2000), 325-335.

[9] L. Osayande and I. Okoli, K_{IC} enhancement for alumina system: a review, *Int. J. App. Ceram. Technol*., 5 (2008), 313–323.

[10] J. Llorca, M. Elices and J. A. Celemin, Toughness and microstructural degradation at high temperature in SiC fiber-reinforced ceramics, *Acta Mater*., 46 (1998), 2441-2453.

[11] F. Yongqing, Y. W. Gu and D. Hejun, SiC whisker toughened Al2O3-(Ti,W)C ceramic matrix composites, *Scripta Mater*., 44 (2001), 111–116.

[12] D. E. Garcıa, S. Schicker, J. Bruhn, R. Janssen and N. Claussen, Processing and mechanical properties of pressureless-sintered niobium–alumina-matrix composites, *J. Am. Ceram. Soc.*, 81 (1998), 429–32.

[13] N. P. Padture, Multifunctional composites of ceramics and single-walled carbon nanotubes, *Adv. Mater*, 21 (2009), 1767–1770.

[14] A. Peigney, Tougher ceramics with nanotubes. *Nature Mater*., 2 (2003), 15–16.

[15] J. Fan, D. Zhao and J. Song, Preparation and microstructure of multi-walled carbon nanotubes toughened Al2O3 composite, *J. Am. Ceram. Soc.*, 89 (2006), 750–753.

[16] C. Laurent, A. Peigney, and A. Rousset, Carbon nanotubes–Fe–Alumina nanocomposites: part II: microstructure and mechanical properties of the hot-pressed composites, *J. Eur. Ceram. Soc.*, 18 (1998), 2005–2013.

[17] G. Zhan, J. Kuntz, J. Wan and K. Mukherjee, Single-walled carbon nanotubes as attractive toughing agent in alumina based nanocomposites, *Nature Mater*., 2 (2003), 38–42.

[18] S. Sarkar and P. K. Das, Microstructure and physicomechanical properties of pressure-less sintered multi-walled carbon nanotube/alumina nanocomposites. *Ceram. Int.* 38 (2012), 423–432.

[19] I. Ahmad, A. Kennedy and Y. Q. Zhu, Carbon nanotubes reinforced alumina nanocomposites: mechanical properties and interfacial investigations. *J. Comp. Sci. and Tech.*, 70 (2010), 1199-1206.

[20] F. Inam, T. Pijis and M. J. Reece. The production of advanced fine-grained alumina by carbon nanotubes addition. *J. Eur. Ceram. Soc.*, 31 (2011), 2853-2859.

[21] I. Ahmad, H. Cao, H. Chen, H. Zhao, A. Kennedy and Y. Q. Zhu, Carbon nanotube toughened aluminium oxide nanocomposites. *J. Eur. Ceram. Soc*., 30 (2009), 865-873.

[22] I. Ahmad, A. Kennedy and Y. Q. Zhu, Wear resistance properties of multi-walled carbon nanotubes reinforced Al2O3 nanocomposite. *Wear*, 269 (2010), 71-78.

[23] Y. C. Fan, L. J. Wang, J. L. Li, J. Q. Li, S. K. Sun, F. Chen, L. D. Chen and W. Jiang, *Carbon*, 48 (2010), 1743–1749. 21.

[24] T. He, J. L. Li, L. J. Wang, J. J. Zhu and W. Jiang, *Mater. Trans*., 50 (2009), 749–751. 22.

[25] C. W. Lam, J. T. James, R. McCluskey, S. Arepalli and R. L. Hunter, *Crit. Rev. Toxicol*., 36 (2006), 189–217.

[26] L. S. Walker and E. L. Corral, Toughness in Grapheme Ceramic Composites, *ACSNANO*, 4 (2011), 3182-3190.

[27] J. Dusza and Balaszi, Microstructure and Farcture Toughness of Si3N4+MLG Platelet Composites, *J. Eur. Ceram. Soc*., 32 (2012), 3389-3397.

[28] K. Wang and T. Wei, Preperation of graphene nanosheets/alumina composites by spark plasma sintering, *Mater. Res. Bulletin*, 46 (2011), 315-318.

[29] L. Jain and H. K. Jiang, Mechanical properties of graphene platelets-reinforced alumina ceramics composites, *Ceram. Inter*., 39 (2013), 6215-6221.

[30] H. Porwal, P. Tatarko, S. Grasso, J. Khaliq, I. Dlouhy and M. J. Reece, Graphene reinforced alumina nano-composites, *Carbon*, 64 (2 0 1 3) 3 5 9 –3 6 9.

[31] H. Porwal, S. Grasso and M. J. Reece, Review of graphene–ceramic matrix composites, *Advances in Applied Ceramics*, 112 (2013), 443-454.

[32] W. S. Hummers and R. E. Offeman, Preparation of Graphitic Oxide *J. Am. Chem. Soc.*, 80 (1958), 1339–1339.

[33] S. Pei and H. Cheng, The reduction of graphene oxide, Carbon, 50 (2012) 3210–3228.

[34] I. Ahmad, M. Islam, A. A. Almajid, B. Yazdani and Y. Q. Zhu, Investigation of yttria-doped Al_2O_3 nanocomposites reinforced by multi-walled carbon nanotubes, *Ceram. Int*., 40 (2014) 9327–9335.

[35] A. Chorfa, M. A. Madjoubi, M. Amidouche, N. Bouras, J. Rubio and F. Rubiom, Glass hardness and elastic modulus determination by nanoindentation using displacement and energy methods, *ceramics – silikáty*, 54 (3) 225-234 (2010).

[36] G. R. Anstis, P. Chantikul and D. B. Marshal, A critical evaluation of indentation technique for measuring fracture toughness: I, direct crack method, *J. Amer. Ceram. Soc*. 64 (1981) 533–538.

[37] H. C. Schniepp, J. L. Li, M. J. McAllister, H. Sai, M. Herrera-Alonso, D. H. Adamson, R. K. Prudhomme, R. Car, D. A. Saville and I. A. Aksay, Functionalized Single Graphene Sheets Derived from Splitting Graphite Oxide. *J. Phys. Chem. B*, 110 (2006), 8535–8539.

[38] H. C. Kim, D. Y. Oh, and I. J. Shon, Sintering of nanophase WC-15 vol% Co hard metals by rapid sintering process, *Int. J. Refract. Hard Mater*., 22 (2004), 197–203.

[39] S. W. Kim and K. A. Khalil, High-frequency induction heat sintering of mechanically alloyed alumina–yttria-stabilized zirconia nano-bioceramics, *J. Am. Ceram. Soc.*, 89 (2006), 1280–1285.

[40] L. Xu, T.B.Ma, Y.Z. Hu, H.Wang, Vanishing stick–slip friction in few-layer graphenes: the thickness effect, *Nanotechnology*, 22 (2011) 285708–285714.

[41] C. Lee, X.Wei, J.W. Kysar, J. Hone, Measurement of the elastic properties and intrinsic strength of monolayer graphene, *Science*, 321 (2008) 385–388.